Article

A SINS/SAR/GPS Fusion Positioning System Based on Sensor Credibility Evaluations

Maoyou Liao [ID] **, Jiacheng Liu, Ziyang Meng** *[ID] **and Zheng You**

Department of Precision Instrument, Tsinghua University, Beijing 100084, China;
liaomy17@mails.tsinghua.edu.cn (M.L.); liu-jc18@mails.tsinghua.edu.cn (J.L.); yz-dpi@mail.tsinghua.edu.cn (Z.Y.)
* Correspondence: ziyangmeng@tsinghua.edu.cn

Abstract: A reliable framework for SINS/SAR/GPS integrated positioning systems is proposed for the case that sensors are in critical environments. Credibility is used to describe the difference between the true error and the initial setting standard deviation. Credibility evaluation methods for inertial measurement unit (IMU), synthetic aperture radar (SAR), and global positioning system (GPS) are presented. In particular, IMU credibility is modeled by noises and constant drifts that are accumulated with time in a strapdown inertial navigation system (SINS). The quality of the SAR image decides the credibility of positioning based on SAR image matching. In addition, a cumulative residual chi-square test is used to evaluate GPS credibility. An extended Kalman filter based on a sensor credibility evaluation is introduced to integrate the measurements. The measurement of a sensor is either discarded when its credibility value is below a threshold or the variance matrix for the estimated state is otherwise adjusted. Simulations show that the final fusion positioning accuracy with credibility evaluation can be improved by 1–2 times compared to that without evaluation. In addition, the derived standard deviation correctly indicates the value of the position error with credibility evaluation. Moreover, the experiments on an unmanned ground vehicle partially verify the proposed evaluation method of GPS and the fusion framework in the actual environment.

Keywords: integrated positioning; credibility evaluation; chi-square test; image matching; Kalman filter; data fusion

1. Introduction

Accurate and reliable positioning is of great significance to aircraft and other high-speed carrier navigation. Various kinds of sensors, including IMU, GPS, and SAR, have been developed for positioning [1–11]. Nevertheless, every sensor has its pros and cons and it is therefore not reliable to depend only on one particular sensor for positioning. Multi-sensor fusion techniques have been commonly introduced to improve the accuracy and reliability of positioning [1].

Strapdown inertial navigation system (SINS) is a system that can continuously solve navigation parameters such as attitude, velocity, and position for a carrier just by integrating the angular velocity and linear acceleration from the IMU fixed on the carrier. Savage [2,3] summarized the numerical integration algorithms of SINS in detail. However, noises of IMU, especially constant drifts, are accumulated in SINS and degrade the positioning accuracy. Therefore, SINS cannot be trusted after a long time when there is no compensation from other sensors. GPS is a suitable sensor to be fused with IMU, since it has high absolute positioning accuracy and positioning error will not accumulate with time [4,7]. Wang et al. propose a robust tightly coupled GNSS/MEMS-SINS navigation approach aided by non-holonomic constraint, and it is shown that the stand-alone accuracy is improved during 60 s GNSS outages [5]. Li et al. proposed a new GPS/INS (inertial navigation system, INS) hybrid method to bridge GPS outages such that reliable and accurate positioning results can be achieved [6]. However, GPS may provide biased, even wrong, positioning results in a complicated electromagnetic environment where the GPS receiver can be easily

attacked by a GPS spoofing agent [12–14]. Guo proposes a covert spoofing algorithm for an unmanned aerial vehicle (UAV) based on GPS/INS navigation system and shows that when the acceleration component of the counterfeit GPS signal is the difference between the UAV's current acceleration and the spoofing control input, the UAV can be covertly spoofed [13]. Narain et al. evaluate the security guarantees of INS-aided GPS tracking and navigation for road transportation systems when the GPS/INS system is attacked by a spoofer [14].

SAR is a remote sensing ground observation technique that can obtain high-resolution radar images under severe weather conditions [15]. SAR images can be used to determine the positioning of a carrier using image matching methods, e.g., the scale invariant feature transform (SIFT) [8,16]. In particular, the authors of [17] propose an improved SIFT framework to reduce the influence of speckle noise for SAR image matching by designing a nonlinear multi-scale space construction strategy. Rai et al. give an insightful technical review of different speckle filtering and enhancement approaches for speckled remote sensing images [18]. Compared with GPS, the SAR image matching method has the advantages of strong anti-interference in critical environments. Therefore, SAR is another suitable sensor that can be integrated with IMU, especially during GPS outages or attacks. Gao et al. propose a robust adaptive filtering method for SINS/SAR integrated navigation systems, which can adaptively adjust the covariance matrix of system state noise according to the adaptive factor constructed by predicted residuals [9]. The authors of [10] propose a multi-sensor data fusion method for an INS/GPS/SAR integrated navigation system that combines local decentralized fusion with global optimal fusion to enhance accuracy and reliability. The authors of [11] analyze the performance of a federated filter for SAR/TRN/GPS/INS (terrain referenced navigation, TRN) integration compared with the centralized integration method. An INS/GPS/SAR incorporated system for target geolocation improvement is simulated through a Kalman filter, and the SAR profits of geolocation precision objectives are analyzed in [19].

In addition to the positioning technique of a single sensor and multi-sensor fusion strategy, the study of the evaluation on the quality of positioning results is also of great importance. In particular, a monitor that uses an inertial navigation system (INS) measurement to detect spoofing attacks on GPS is described in [12]. Gao et al. propose a random weighting method to estimate white noise errors in SINS/GPS/SAR integrated navigation systems and achieve higher accuracy than the least-squares method [20]. Zhao proposes credibility evaluation methods based on the fuzzy reasoning model of SAR image matching results and the proposed methods are used in an INS/SAR adaptive Kalman filtering algorithm [21]. In general, most of the integrated positioning methods focus mainly on the fusion of information from reliable sensors. However, when the carrier is in a critical environment or suffered from serious external interference, a bias or even error will emerge in the positioning results of certain sensors [12]. Therefore, it is necessary to evaluate the positioning results of sensors to eliminate the measurements with serious errors or correct the positioning results with biases or errors.

Motivated by the above observations, this paper proposes a multi-sensor fusion framework for positioning based on sensor credibility evaluations. We first evaluate the credibilities of IMU, SAR, and GPS from their respective sensors. The positioning results are then integrated into an extended Kalman filter based on the credibility evaluations. The main contributions of this paper are two-fold. In the first place, customized methods are proposed for the credibility evaluations of IMU, SAR, and GPS based on each sensor's characteristics. In the second place, an SINS/SAR/GPS fusion framework is proposed based on sensor credibility evaluations and is shown to obtain more accurate and reliable positioning results in critical environments.

The remaining sections of this paper are organized as follows. System model, sensor models and problems to be solved are described in Section 2. Estimator design and methods for evaluating each sensor's credibility are presented in Section 3. Simulations and experiments are carried out in Section 4 to verify the designed estimator and proposed credibility evaluation methods. Conclusions are drawn in Section 6.

Notations: In what follows, *n* denotes the positioning reference frame, with ENU (East-North-Up) pointing orientations; *b* denotes carrier's body frame, with X-Right, Y-Forward, and Z-Up pointing orientations; *e* denotes the earth-centered-earth-fixed (ECEF) frame; *i* denotes the inertial frame whose origin is situated at the center of mass of the earth. IMU is fixed on the carrier, we can transform the IMU body frame to the carrier's body frame (the frame *b*) easily once we know the external parameters between the IMU and the carrier. Therefore, in the remaining parts of this paper, we no longer distinguish the IMU body frame and the carrier's body frame, and the two are regarded as the same frame. For $x = [x_1, x_2, x_3]^T$, define $x^\times$ as a skew-symmetric matrix, namely,

$$x^\times = \begin{bmatrix} 0 & -x_3 & x_2 \\ x_3 & 0 & -x_1 \\ -x_2 & x_1 & 0 \end{bmatrix}.$$

2. Problem Statement

2.1. System Model

In general, SINS is used as the dynamics model of the carrier since prior kinematic information of the carrier is normally unknown or subject to uncertainties. The ENU frame is chosen as the positioning reference frame of SINS, which means that SINS can solve the position and attitude of the IMU body frame (also the frame *b*) in the ENU frame. Since the state equations in the SINS algorithm are non-linear, we choose the error model of SINS as the system state model [4]:

$$\dot{x}(t) = F(t)x(t) + G(t)\xi(t), \tag{1}$$

where $x(t)$ is the system incremental state vector, $F(t)$ is the dynamic matrix, $\xi(t)$ is the system noise and assumed to be a white Gaussian process, $G(t)$ is the noise coefficient matrix.

The system incremental state vector $x(t)$ is defined as:

$$x = [\phi^T \ (\delta v^n)^T \ (\delta p^e)^T \ (\varepsilon^b)^T \ (\nabla^b)^T]^T$$

where ϕ is the attitude error represented by a 3x1 misalignment angle vector, $\delta p^e = [\delta L, \delta \lambda, \delta h]^T$ is the position error in ECEF frame (*L*, λ, *h* denote longitude, latitude, and altitude, respectively.), $\delta v^n = [\delta v_E, \delta v_N, \delta v_U]^T$ is the velocity error in the positioning reference frame, ε^b and ∇^b are constant biases of gyroscope and accelerometer in IMU. Note that the error here means a correction to the nominal value of the corresponding state. For example, if the no nominal value of the position is $\bar{p}^e$, then the true value of the position is $p^e = \bar{p}^e + \delta p^e$.

The detailed expressions of matrices $F(t)$ and $G(t)$ can be found in Equation [4] as:

$$F(t) = \begin{bmatrix} -(\omega_{ie}^n + \omega_{en}^n)^\times & M_{av} & M_{ap} & -C_b^n & 0_{3\times3} \\ (C_b^n f^b)^\times & M_{vv} & M_{vp} & 0_{3\times3} & C_b^n \\ 0_{3\times3} & M_{pv} & M_{pp} & 0_{3\times3} & 0_{3\times3} \\ 0_{6\times3} & 0_{6\times3} & 0_{6\times3} & 0_{6\times3} & 0_{6\times3} \end{bmatrix},$$

$$G(t) = \begin{bmatrix} -C_b^n & \mathbf{0}_{3\times3} \\ \mathbf{0}_{3\times3} & C_b^n \\ \mathbf{0}_{9\times3} & \mathbf{0}_{9\times3} \end{bmatrix},$$

where,

$$M_{av} = \begin{bmatrix} 0 & -1/R_{Mh} & 0 \\ 1/R_{Nh} & 0 & 0 \\ \tan L/R_{Nh} & 0 & 0 \end{bmatrix},$$

$$M_{ap} = M_1 + M_2,$$

$$M_{vv} = (v^n)^\times M_{av} - (2\omega_{ie}^n + \omega_{en}^n)^\times,$$

$$M_{vp} = (v^n)^\times (2M_1 + M_2),$$

$$M_1 = \begin{bmatrix} 0 & 0 & 0 \\ -\omega_{ie}\sin L & 0 & 0 \\ \omega_{ie}\cos L & 0 & 0 \end{bmatrix},$$

$$M_2 = \begin{bmatrix} 0 & 0 & v_N/R_{Mh}^2 \\ 0 & 0 & -v_E/R_{Nh}^2 \\ v_E\sec^2 L/R_{Nh} & 0 & -v_E\tan L/R_{Nh}^2 \end{bmatrix},$$

$$M_{pv} = \begin{bmatrix} 0 & 1/R_{Mh} & 0 \\ \sec L/R_{Nh} & 0 & 0 \\ 0 & 0 & 1 \end{bmatrix},$$

$$M_{pp} = \begin{bmatrix} 0 & 0 & -v_N/R_{Mh}^2 \\ v_E\sec L\tan L/R_{Nh} & 0 & -v_E\sec L/R_{Nh}^2 \\ 0 & 0 & 0 \end{bmatrix},$$

$$\omega_{en}^n = [-v_N/R_{Mh}, v_E/R_{Nh}, v_E\tan L/R_{Nh}]^T,$$

$$R_{Mh} = R_M + h, \ R_{Nh} = R_N + h,$$

$$R_M = \frac{R_e(1-e^2)}{(1-e^2\sin^2 L)^{3/2}}, \ R_N = \frac{R_e}{\sqrt{1-e^2\sin^2 L}},$$

and R_e is the earth's semimajor axis, e is the earth's eccentricity, ω_{ie} is the earth's angular rate, ω_{ie}^n is the earth's angular rate vector projection in the ENU frame, C_b^n is the transformation matrix from b-frame to n-frame.

2.2. Models of Sensors

2.2.1. IMU

The IMU consists of a triaxial accelerometer and a triaxial gyroscope. We assume that the systematic errors of IMU have been calibrated in advance, including misalignment and scale factor inaccuracy. To establish a feasible IMU model, it is suggested to use a constant drift model that compromises between the model precision and model complexity considering the random errors of IMU [2,3]:

$$\omega_{ib,\mathrm{IMU}}^b = \omega_{ib}^b + \varepsilon^b + \eta_\omega, \tag{2}$$

$$f_{\mathrm{IMU}}^b = f^b + \nabla^b + \eta_f, \tag{3}$$

where ω_{ib}^b denotes the theoretical angular velocity relative to the i-frame of the carrier in the b-frame, $\omega_{ib,\mathrm{IMU}}^b$ is the measurement obtained from the gyroscope, f^b denotes the theoretical specific force in b-frame, f_{IMU}^b is the measurement obtained from accelerometer, ε^b and ∇^b are constant biases of gyroscope and accelerometer, η_ω and η_f are the measurement noises and assumed to be white Gaussian processes.

2.2.2. GPS

GPS continuously outputs the geographic coordinate in the ECEF frame of the receiver's antenna phase center. It can be easily transformed to the carrier's position, denoted by p_{gps}^e. During certain time intervals, the carrier might be in a critical or complicated environment, resulting in biased GPS outputs. Therefore, the measurement model of GPS can be modeled by:

$$p_{gps}^e = p^e + p_{bias} + \eta_{gps}, \tag{4}$$

where $p^e = [L, \lambda, h]^T$ is the theoretical position of the carrier in the ECEF frame, p_{gps}^e is the measurement obtained from GPS, p_{bias} is the position bias caused by attacks or critical environment, and η_{gps} is the measurement noise and assumed to be a white Gaussian process.

2.2.3. SAR

The carrier's longitude (L_{SAR}), and latitude (λ_{SAR}) can be obtained from the SAR image matching method. With the altitude (h_{alt}) obtained from the altimeter, we can obtain the carrier's position in the ECEF frame, i.e., $p_{SAR}^e = [L_{SAR}, \lambda_{SAR}, h_{alt}]^T$. However, unlike GPS, which can continuously obtain positioning information throughout the entire trajectory, SAR only provides a single point positioning when the carrier passes the matching area. In those matching areas, the measurement model of SAR is:

$$p_{SAR}^e = p^e + \eta_{SAR}, \tag{5}$$

where p_{SAR}^e is the measurement obtained from SAR&Altimeter, η_{SAR} is the measurement noise and assumed to be a white Gaussian process.

2.3. Objective

When the carrier is in a critical environment or suffers from serious external interference, biases or even errors will emerge in the positioning results of a sensor, which entails that the measurement variance $R = E[\eta\eta^T]$ of the sensor cannot correctly indicate the confidence of the error. This implies that:

$$R \neq E[(z - z_{true})(z - z_{true})^T], \tag{6}$$

where z is the measurement obtained from a sensor, z_{true} is the theoretical true value of the measurement. Therefore, we evaluate the credibility of a sensor using:

$$C := f_c(\|R - E[(z - z_{true})(z - z_{true})^T]\|), \tag{7}$$

where $f_c(\cdot)$ is a monotone increasing function which ranges from 0 to 100%. However, since we can not get the theoretical true value of a sensor's measurement, Equation (7) is just a definition and the credibility evaluation method of a sensor can be derived according to the characteristics of the sensor's errors.

Based on the discussions given in this section, we know that the position calculated by SINS alone can only be accurate and reliable in a short time due to the constant drift. GPS will be biased or even completely wrong in certain time intervals due to the critical environment or attacks. In addition, SAR can only provide discrete single-point positioning. Therefore, it is necessary to evaluate measurements of the SINS/SAR/GPS at all times before integrating the positioning results. Depending on the evaluation results, the SINS/SAR/GPS positioning results are integrated more reliably.

3. Materials and Methods

We propose a SINS/SAR/GPS fusion framework based on sensor credibility evaluations and the system diagram is shown in Figure 1. Using the measurements from IMU, SAR/Altimeter, and GPS, we can get the positioning results of a carrier by SINS, image matching methods, and GPS positioning algorithm, respectively. The credibilities (ranging from 0 to 100%) of each sensor are then obtained using the proposed evaluation methods (stated in Section 3.2. The information is discarded if the corresponding credibility is below a certain threshold and the measurement covariance matrix is appropriately adjusted when the corresponding credibility exceeds this threshold. The positioning results after credibility evaluations are finally integrated into an extended Kalman filter to get the ultimate position of the carrier. The ultimate positioning result of the filter is fed back to the SINS to correct errors caused by the accumulated drifts and noises, and is also fed back to the credibility evaluation of GPS as a reference.
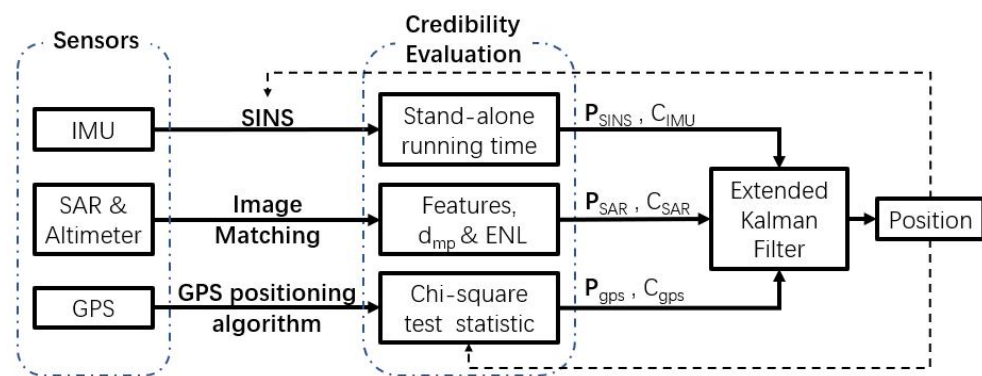

Figure 1. SINS/SAR/GPS credibility fusion positioning framework.

3.1. Extended Kalman Filter Estimator

In this section, we describe a tightly-coupled extended Kalman filter (EKF) estimator based on sensor credibility evaluations to integrate the positioning results of SINS/GPS/SAR.

3.1.1. Time Update

The filter estimator uses an SINS error model as the state prediction model. Employing a first-order Euler integration to Equation (1), the discrete form of the state prediction model can be written as:

$$x_{k/k-1} = \Phi_{k/k-1} x_{k-1} + \Gamma_{k-1} \zeta_{k-1}, \tag{8}$$

$$P_{k/k-1} = \Phi_{k/k-1} P_{k-1} \Phi_{k/k-1}^T + \Gamma_{k-1} Q_{k-1} \Gamma_{k-1}^T, \tag{9}$$

where $\Phi_{k/k-1}$ is the state transition matrix, $\Gamma_{k-1} \approx G(t_{k-1})$ is the noise coefficient matrix, $P_{k/k-1}$ is the pre-measurement state estimate error covariance matrix, $Q_{k-1} = E[\zeta_{k-1} \zeta_{k-1}^T]$ is the process noise variance matrix, and ζ_k is the system noise. By considering $T_s = t_k - t_{k-1}$ as the time interval of discretization and assuming it sufficiently small, we can take an approximation in the calculation of $\Phi_{k/k-1}$, that is $\Phi_{k/k-1} \approx I + F(t_{k-1})T_s$.

3.1.2. Measurement Update

For the positioning result p_{gps}^e from GPS, we take the difference between the position p_{SINS}^e calculated by SINS and p_{gps}^e as the measurement equation:

$$z_{gps} = p_{SINS}^e - p_{gps}^e = H_{gps} x + \eta_{gps}, \tag{10}$$

where $H_{gps} = [0_{3\times6} \ I_{3\times3} \ 0_{3\times6}]$ is the measurement matrix, η_{gps} is the measurement error vector, and $R_{gps} = E[\eta_{gps} \eta_{gps}^T]$ is the corresponding measurement variance matrix.

Similarly, the measurement equation for p^e_{SAR} is:

$$z_{\text{SAR}} = p^e_{\text{SINS}} - p^e_{\text{SAR}} = H_{\text{SAR}}x + \eta_{\text{SAR}}, \tag{11}$$

where $H_{\text{SAR}} = [\mathbf{0}_{3\times6}\ I_{3\times3}\ \mathbf{0}_{3\times6}]$ is the measurement matrix, η_{SAR} is the measurement error vector, and $R_{\text{SAR}} = E[\eta_{\text{SAR}}\eta^T_{\text{SAR}}]$ is the corresponding measurement variance matrix.

The final measurement equation of the filter will be adjusted according to the credibility of GPS and SAR, denoted by C_{gps} and C_{SAR}, respectively.

(a) When GPS and SAR are both partially reliable (meaning $C_{\text{th,g}} \leq C_{\text{gps}} \leq 100\%$ and $C_{\text{th,s}} \leq C_{\text{SAR}} \leq 100\%$ ($C_{\text{th,g}}$, $C_{\text{th,s}}$ are pre-given thresholds)), the measurement of the filter is the combination of Equations (10) and (11):

$$z = \begin{bmatrix} z_{\text{gps}} \\ z_{\text{SAR}} \end{bmatrix} = \begin{bmatrix} H_{\text{gps}} \\ H_{\text{SAR}} \end{bmatrix}x + \begin{bmatrix} \gamma_{\text{gps}} \\ \gamma_{\text{SAR}} \end{bmatrix}, \tag{12}$$

where γ_{gps} and γ_{SAR} are measurement error vectors adjusted according to the credibility values of GPS and SAR. As $R_{\text{gpsc}} = E[\gamma_{\text{gps}}\gamma^T_{\text{gps}}]$ and $R_{\text{SARc}} = E[\gamma_{\text{SAR}}\gamma^T_{\text{SAR}}]$ are the corresponding measurement variance adjusted matrices, we next specify γ_{gps} and γ_{SAR} by those two variance matrices.

Since the noise is assumed to be a white Gaussian process, the standard deviation $\sigma_{\text{x}} = \sqrt{R_{\text{x}}}$ (subscript x denotes gps or SAR) completely describes the noise distribution. This means that the probability of the true measurement value in $z_{\text{x}} \pm \sigma_{\text{x}}$ is:

$$f_{\text{norm}}(1) - f_{\text{norm}}(-1) = 0.6827,$$

where $f_{\text{norm}}(\cdot)$ is the standard normal distribution function. If the credibility of the sensor is less than 100%, the probability decreases to $0.6827C_{\text{x}}$. Therefore, we can infer that the variance matrix after credibility correction should be:

$$\sqrt{R_{\text{gpsc}}} = \sqrt{R_{\text{gps}}}/f^{\text{inv}}_{\text{norm}}(0.6827C_{\text{gps}}/2 + 0.5), \tag{13}$$

$$\sqrt{R_{\text{SARc}}} = \sqrt{R_{\text{SAR}}}/f^{\text{inv}}_{\text{norm}}(0.6827C_{\text{SAR}}/2 + 0.5), \tag{14}$$

where $f^{\text{inv}}_{\text{norm}}(\cdot)$ is the inverse function of the standard normal distribution.

(b) When only GPS is reliable (meaning $C_{\text{th,g}} \leq C_{\text{gps}} \leq 100\%$ and $C_{\text{SAR}} < C_{\text{th,s}}$), the measurement of the filter is:

$$z = z_{\text{gps}} = H_{\text{gps}}x + \gamma_{\text{gps}}. \tag{15}$$

(c) When only SAR is reliable (meaning $C_{\text{th,s}} \leq C_{\text{SAR}} \leq 100\%$ and $C_{\text{gps}} < C_{\text{th,g}}$), the measurement of the filter is:

$$z = z_{\text{SAR}} = H_{\text{SAR}}x + \gamma_{\text{SAR}}. \tag{16}$$

(d) When neither GPS or SAR are reliable, the measurement update will not be executed.

With the system state prediction in Equation (8) and employing discretization to the measurement Equations (12), (15), and (16), the proposed extended Kalman filter estimator can be summarized as:

Time Update:

$$\begin{cases} \hat{x}_{k/k-1} = \Phi_{k/k-1}\hat{x}_{k-1}, \\ P_{k/k-1} = \Phi_{k/k-1}P_{k-1}\Phi_{k/k-1}^T + \Gamma_{k-1}Q_{k-1}\Gamma_{k-1}^T, \end{cases}$$

Measurement Update:

$if\ C_{\text{gps}}<C_{\text{th,g}},\ C_{\text{SAR}}<C_{\text{th,s}}$

$\quad goto\ $ Time Update

$elseif\ C_{\text{th,g}}\leq C_{\text{gps}}\leq 100\%,\ C_{\text{SAR}}<C_{\text{th,s}}$

$\quad z_k = z_{\text{gps},k},\ H_k = H_{\text{gps},k},\ R_k = R_{\text{gpsc},k}$

$elseif\ C_{\text{gps}}<C_{\text{th,g}},\ C_{\text{th,s}}\leq C_{\text{SAR}}\leq 100\%$

$\quad z_k = z_{\text{SAR},k},\ H_k = H_{\text{SAR},k},\ R_k = R_{\text{SASRc},k}$

$elseif\ C_{\text{th,g}}\leq C_{\text{gps}}\leq 100\%, C_{\text{th,s}}\leq C_{\text{SAR}}\leq 100\%$

$$z_k = \begin{bmatrix} z_{\text{gps},k} \\ z_{\text{SAR},k} \end{bmatrix},\ H_k = \begin{bmatrix} H_{\text{gps},k} \\ H_{\text{SAR},k} \end{bmatrix},$$

$$R_k = \begin{bmatrix} R_{\text{gpsc},k} & 0 \\ 0 & R_{\text{SASRc},k} \end{bmatrix},$$

(where R_{gpsc} and R_{SARc} can be calculated by Equations (13) and (14))

$$\begin{cases} K_k = P_{k/k-1}H_k^T(H_k P_{k/k-1}H_k^T + R_k)^{-1} \\ \hat{x}_k = \hat{x}_{k/k-1} + K_k(z_k - H_k\hat{x}_{k/k-1}) \\ P_k = (I - K_k H_k)P_{k/k-1} \end{cases},$$

where $\hat{x}_{k/k-1}$ is the a priori estimate of state x, $\hat{x}_k$ is the post estimate of state x, P_k is the post-measurement state estimate error covariance matrix.

3.2. Sensors' Credibility Evaluation

3.2.1. IMU

Since IMU is used in the state prediction model, the errors of SINS caused by the accumulated drifts and noises can be corrected by the feedback positioning result from the filter. We therefore assume that the credibility of IMU is 100% in this work. When IMU is not used in the state prediction model, the credibility of IMU should be evaluated as a measurement sensor. The position and attitude calculated by SINS is the joint integral of acceleration and angular velocity from IMU over time. Therefore, the error of the position calculated by SINS will increase with time due to the noise and constant drift of IMU. In other words, the credibility of IMU will decrease with time. Based on the above analysis, we evaluate the credibility of IMU as:

$$C_{\text{IMU}} = f_{\text{IMU}}(\triangle t) = \begin{cases} 1 - ((t - t_0)/T)^k, & \triangle t < T \\ 0, & \triangle t \geq T \end{cases}' \tag{17}$$

where $\triangle t = t - t_0$ is the period when only SINS is performed, and t_0 is the starting epoch. If any other global position information is used to correct SINS in epoch t_a, we can set $t_0 = t_a$. In addition, T and k are the parameters which will be set according to the performance of IMU. In particular, small drift and high accuracy of IMU corresponds to large values of T and k. The value of k usually ranges within 2.5~3.0.

3.2.2. SAR

The quality of SAR images has a great influence on the accuracy of positioning result using image matching methods. Due to the atmospheric refraction, topography, and other environmental factors, deformation and speckle noise will occur in SAR images. An SAR credibility evaluation method based on the fuzzy reasoning model is described in [21].

Motivated by this work, we chose the number of successfully matched features between the reference SAR image and the real-time SAR image, the mean of pixel-offset after affine transformation, and the equivalent number of looks (ENL) of the SAR image, to evaluate the credibility of positioning result of the SAR image matching method. The framework of the SAR credibility evaluation is shown in Figure 2.
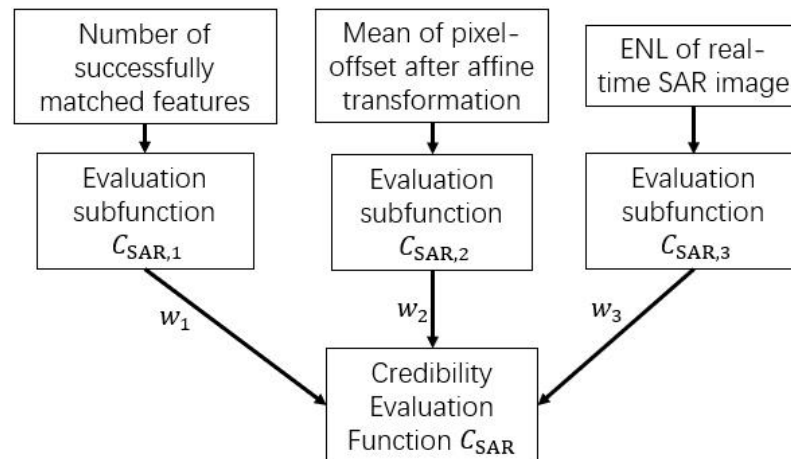

Figure 2. SAR credibility evaluation.

In particular,

(a) $C_{\text{SAR},1}$ is determined by the number of successfully matched features:

$$C_{\text{SAR},1} = \begin{cases} n/N, & n \leq N \\ 1, & n > N \end{cases},$$

(18)

where n is the number of successfully matched features, N is the parameter which will be set according to the total number of features that can be extracted from the image.

(b) $C_{\text{SAR},2}$ is determined by the mean of the pixel-offset after the affine transformation:

$$C_{\text{SAR},2} = \begin{cases} 1 - d_{\text{mp}}/D, & d_{\text{mp}} \leq D \\ 0, & d_{\text{mp}} > D \end{cases},$$

(19)

where d_{mp} is the the mean of the pixel-offset, and D is a pre-given parameter.

(c) $C_{\text{SAR},3}$ is determined by the ENL of the SAR image:

$$C_{\text{SAR},3} = \begin{cases} \text{ENL}/P, & \text{ENL} \leq P \\ 1, & \text{ENL} > P \end{cases},$$

(20)

where ENL is an index of the relative intensity of speckle noise in the SAR image, and P is a pre-given parameter. Generally speaking, the larger the ENL, the weaker the speckle noise in the image [15].

With Equations (18), (19), and (20), we can get the ultimate credibility evaluation function of the SAR image matching positioning:

$$C_{\text{SAR}} = w_1 C_{\text{SAR},1} + w_2 C_{\text{SAR},2} + w_3 C_{\text{SAR},3},$$

(21)

where w_1, w_2, w_3 are weight coefficients, and satisfy the relation $w_1 + w_2 + w_3 = 100\%$.

3.2.3. GPS

The accuracy of GPS is affected by many factors including signal strength, the number of satellites received, and also potential attacks from GPS spoofing agents. Therefore, it is necessary to combine external auxiliary sensor information to evaluate the credibility of GPS positioning results. An INS-monitor-based chi-square test is used to detect spoofing attacks on the GPS receiver in [12]. Motivated by this work, we performed a credibility evaluation based on the cumulative residual chi-square test.

(a) The residual vector r_k of the GPS measurement in the extended Kalman filter, at time epoch k, is defined as:

$$r_k = z_{\text{gps},k} - H_{\text{gps},k}\hat{x}_{k/k-1},\qquad(22)$$

where $\hat{x}_{k/k-1}$ is the a priori estimate of state x at time epoch k.

(b) Calculate the single-point chi-square test statistic u_k with the residual vector:

$$u_k = r_k^T S_k^{-1} r_k,\qquad(23)$$

where $S_k = H_{\text{gps},k}P_{k/k-1}H_{\text{gps},k}^T + R_{\text{gps},k}$ is the covariance matrix of the residual vector at time epoch k.

(c) The cumulative test statistic is defined as the sum of single-point chi-square test statistics from u_{k-m+1} to u_k:

$$U_k = \sum_{i=k-m+1}^{k} u_i.\qquad(24)$$

(d) Set a threshold T_d. Then, the credibility evaluation function of GPS is defined as:

$$C_{\text{gps}} = \begin{cases} 1, & U_k \leq T_d \\ \frac{3}{2} - \frac{U_k}{2T_d}, & T_d < U_k < 3T_d. \\ 0, & U_k > T_d \end{cases}\qquad(25)$$
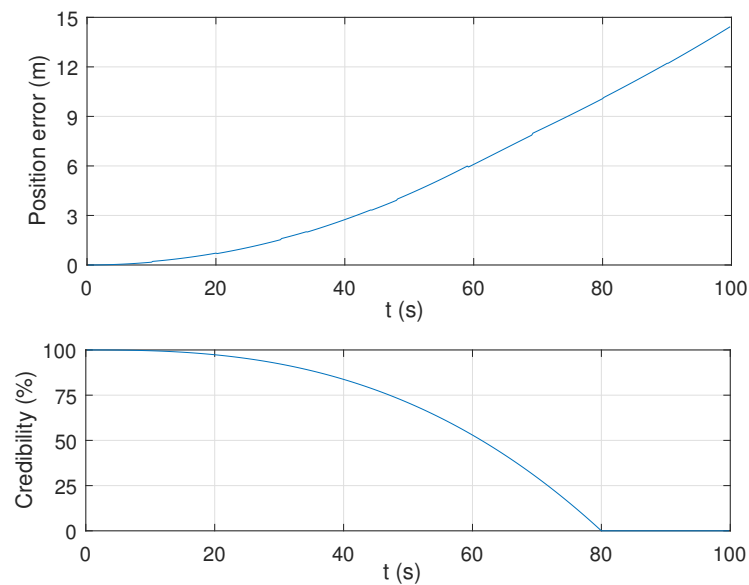
4. Results

4.1. Simulation Verification

In this section, simulations are carried out in MATLAB to verify the credibility evaluation methods and the proposed estimator.

4.1.1. Credibility Evaluation for IMU

IMU simulator generates accelerometer and gyroscope data with noise at a frequency of 100 Hz. The gyroscope constant drift error is $\varepsilon^b = [0.015, 0.015, 0.015]^T \, ^\circ/\text{h}$, gyroscope angular random walk coefficient is $\varepsilon_w^b = [0.001, 0.001, 0.001]^T \, ^\circ/\sqrt{\text{h}}$, accelerometer constant bias is $\nabla^b = [200, 200, 200]^T \text{ug}$, and accelerometer velocity random walk coefficient is $\nabla_w^b = [3, 3, 3]^T \text{ug}/\sqrt{\text{Hz}}$. SINS algorithm is executed to obtain the position of the carrier. The whole flight process takes 100 s. The absolute position error of SINS and the credibility of IMU were evaluated according to the method described in Section 3.2 (the parameters are set as $T = 80$ and $k = 2.62$), and are shown in Figure 3. It is shown that the trajectory of the IMU's credibility agreed with the absolute position error of SINS, and the credibility of IMU was above 80% within 40 s.

Figure 3. Position error of SINS and credibility evaluation result of IMU.

4.1.2. Credibility Evaluation for SAR Image Matching

Two SAR images with overlapping areas taken at different times were downloaded from Sandia National Laboratory (http://www.sandia.gov/, accessed on 21 March 2021). One of these two SAR images was used as the reference image and the other as the real-time image. As SAR images are mostly damaged by signal dependent speckle noise, image enhancement and filtering to suppress the speckle noise [17,18] were performed on the two SAR images before matching. Firstly, to deal with the low image contrast and dim brightness of SAR images, the contrast limited adaptive histogram equalization (CLAHE) method [22] was used for image enhancement, which not only improves the sharpness of the image and makes the image features clearer but also limits the contrast of each local histogram and effectively avoids the noise amplification. Secondly, it is shown that the scattering characteristics of almost all practical targets and speckle noise with uneven brightness distribution appear in the original and enhanced SAR images. Therefore, an image filter (e.g., the median filter) was conducted to enhance image quality. Two kinds of algorithms were used to extract the point features in both the reference and real-time SAR images for image matching, i.e., the scale invariant feature transform (SIFT) and the speeded-up robust features (SURF) [17]. By modeling the coordinate transformation as an affine transformation between the reference and real-time SAR images, we eliminate the outliers in a random sample consensus (RANSAC) framework [23]. Then, the affine matrix is re-solved through a linear least square problem using all inliers. Note that we also calculated the average re-projected pixel-offset among all inliers.

The result of image matching is shown in Figure 4. According to the credibility evaluation method of SAR image matching described in Section 3.2, the credibility results are listed in Table 1. From Table 1, it follows that the credibility of the positioning result of SAR image matching using SIFT algorithm (89.6%) was higher than that using the SURF algorithm (81.3%) because SIFT algorithm can get more successfully matched features and smaller pixel-offset.
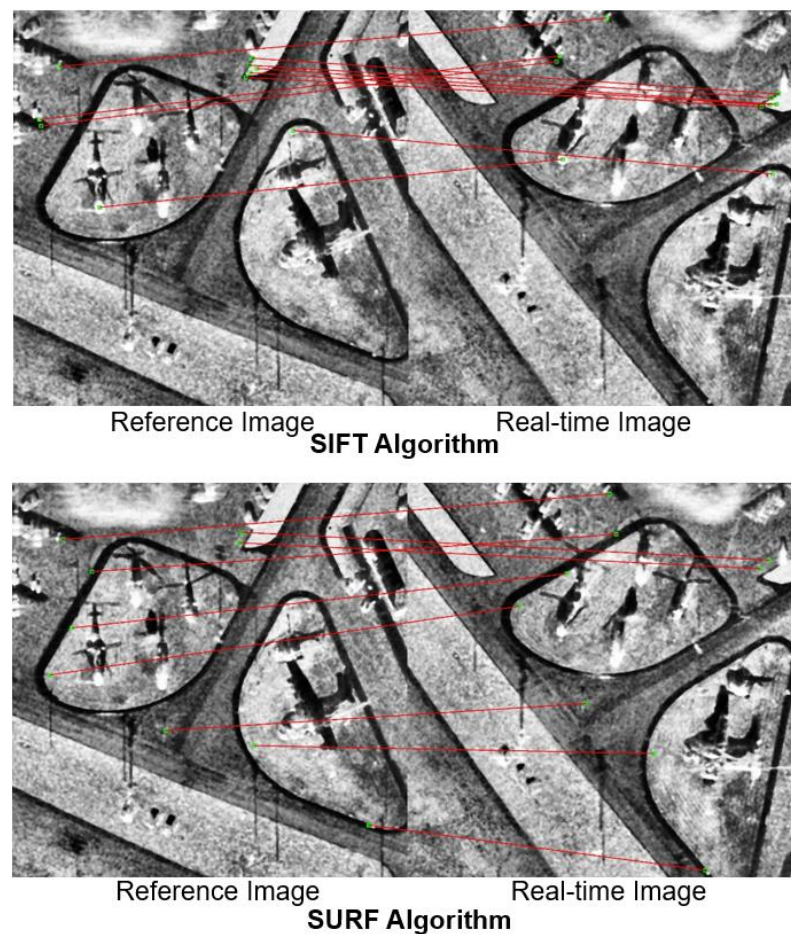
Figure 4. Image matching between SAR images.

Table 1. Credibility of Image Matching between SAR images.

Algorithm	Mean of Pixel-Offset	ENL	Number of Features	Credibility
SIFT	2.28	4.17	10	89.6%
SURF	2.93	4.17	9	81.3%

We also performed the image matching between a real-time SAR image and an optical image as a reference [24]. The optical image was downloaded from Google Maps. We selected a tile of the optical image and converted it to a gray-scale image as the reference image. Image enhancement and filtering were also performed on the real-time SAR image before matching. The result of image matching between SAR and optical images is shown in Figure 5. The credibility results are list in Table 2. According to Figure 5 and Table 2, we know that the credibility evaluation method of SAR image matching is also effective when it is performed between SAR and optical images. We can also see that the credibility of SAR image matching using the SIFT algorithm (80.3%) was higher than that using the SURF algorithm (71.7%). However, when we select an area that is full of buildings and perform the image matching algorithm between SAR and optical images on this area, a wrong image matching result happened as shown in Figure 6. This is because the SAR image is too blurry and distorted to find the correct feature points. The number of successfully matched features was zero, the ENL of the SAR image was 3.23, the pixel-offset after affine transformation was 3.59 (in SIFT algorithm), and the credibility value was 16.1% (This is meaningless as the matching is wrong.). Obviously, when a wrong image matching result happens, the credibility value is low.
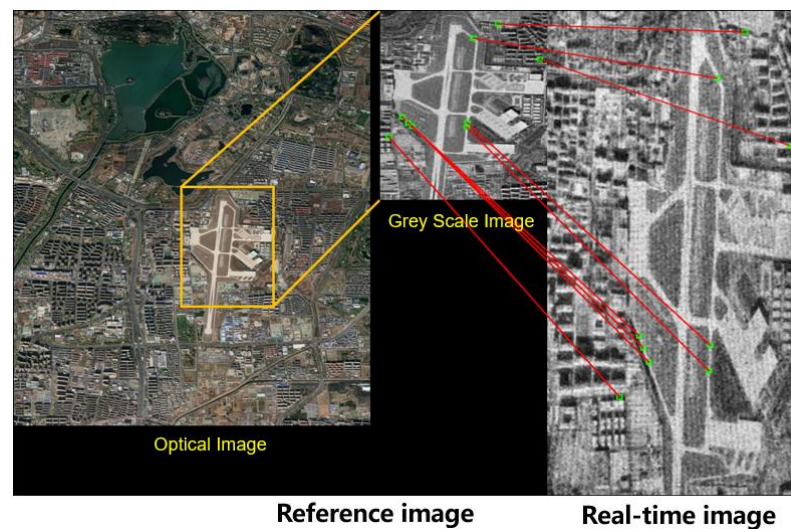
Figure 5. Image matching between SAR and optical images.

Table 2. Credibility of Image Matching between SAR and optical images.

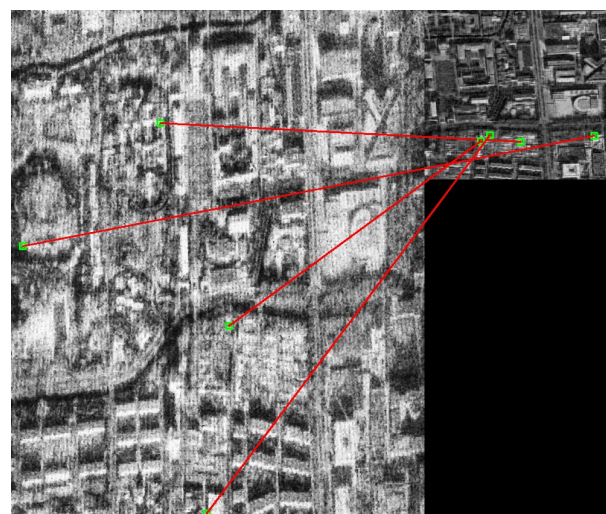| Algorithm	Mean of Pixel-Offset	ENL	Number of Features	Credibility
SIFT	3.37	4.02	9	80.3%
SURF	4.16	4.02	8	71.7%

Figure 6. Failed image matching between SAR and optical images.

4.1.3. Credibility Evaluation of GPS Measurements

A GPS simulator was used to generate position with noise and bias of the carrier at a frequency of 1 Hz. The noise was set as a white Gaussian process with zero mean and standard deviation $\sigma_{\mathrm{gps}} = 10$ m and the bias caused by attacks was added in three particular time intervals of 200 s, including 150 s–350 s, 562 s–762 s, and 974–1174 s. The position error and bias generated by the GPS simulator are shown in Figure 7 and the trajectory generated by the GPS simulator is shown by the dashed green line in Figure 8.

The credibility of positioning results generated by the GPS simulator was evaluated according to the method described in Section 3.2 and are shown in Figure 9. Compared with the time intervals without bias, it can be found that when the bias added to the GPS positioning result exceeds about 20 m, the credibility of GPS drops to zero.
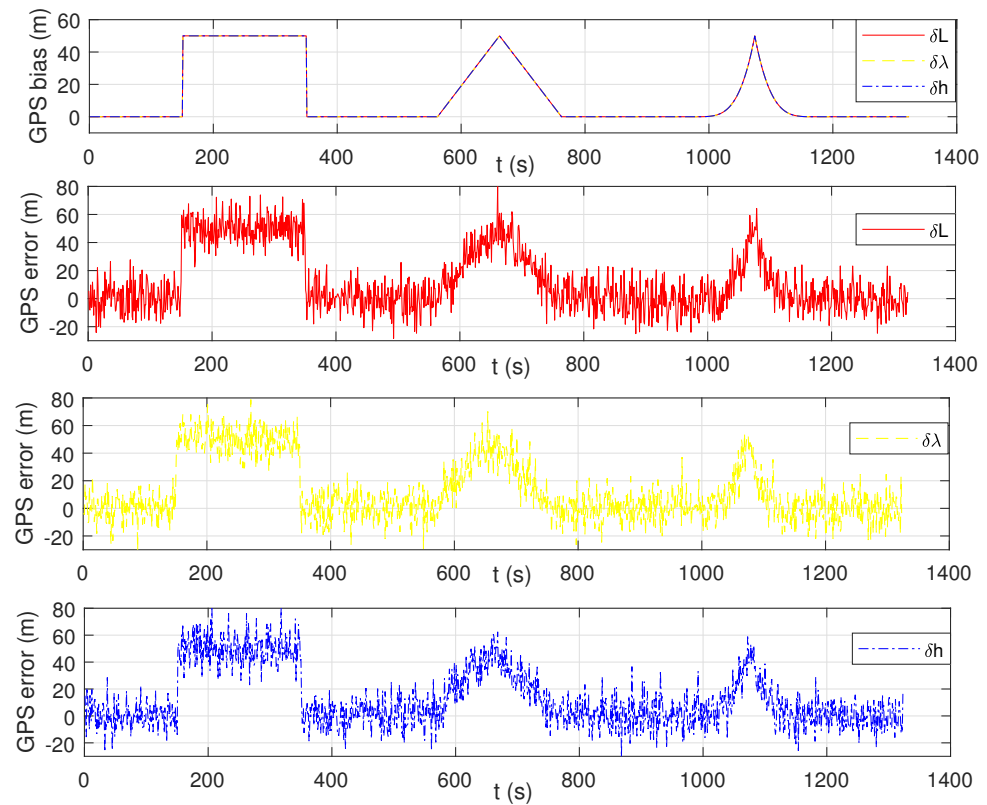

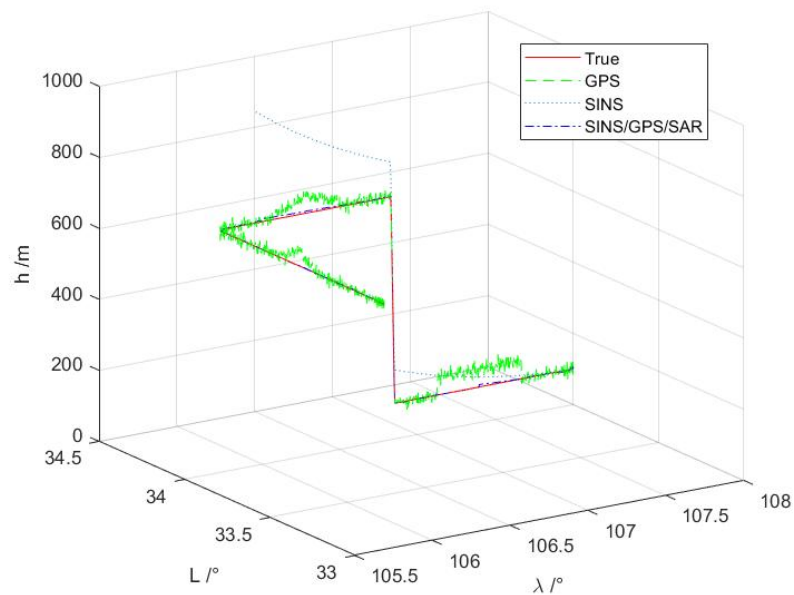**Figure 7.** Position error and bias generated by GPS simulator.
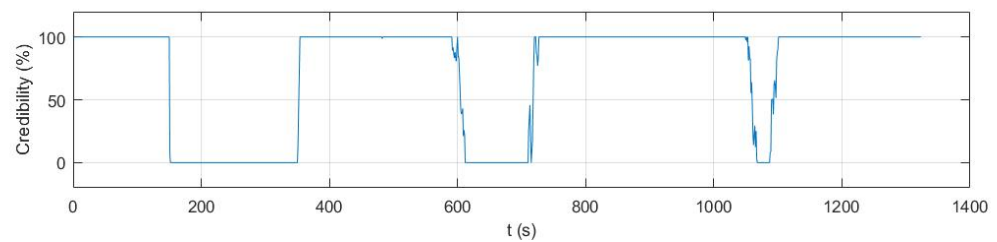

Figure 8. 3D trajectory tracking.

Figure 9. Credibility evaluation result of GPS.

4.1.4. Proposed Estimator Based on Sensors' Credibility Evaluations

We used a flight track generator to generate real flight trajectory data of the carrier, including attitude, position, and velocity of the carrier. The initial position of the carrier was $\boldsymbol{p}_0^e = [L_0, \lambda_0, h_0]^T = [34°, 108°, 100 \text{ m}]^T$. The initial velocity was 100 m/s heading west. This means that $\boldsymbol{v}_0^n = [v_E, v_N, v_U]^T = [-100, 0, 0]^T$ m/s, and the initial attitude is $A_0 = [0, 0, 90°]^T$ using an Euler angle (3-1-2) representation. The whole flight process takes 1324 s, and the flight trajectory is shown by the solid red line in Figure 8.

The IMU simulator generates accelerometer and gyroscope data with noise according to the constant drift model at a frequency of 100 Hz. The gyroscope constant drift error was $\boldsymbol{\varepsilon}^b = [0.015, 0.015, 0.015]^T$ °/h, gyroscope angular random walk coefficient was $\boldsymbol{\varepsilon}_w^b = [0.001, 0.001, 0.001]^T$ °/$\sqrt{\text{h}}$, accelerometer constant bias was $\nabla^b = [90, 90, 90]^T$ ug, and accelerometer velocity random walk coefficient was $\nabla_w^b = [1, 1, 1]^T$ ug/$\sqrt{\text{Hz}}$. The SINS algorithm was executed to obtain the position and attitude of the carrier. The earth's semimajor axis is R_e = 6,378,137 m, the earth's eccentricity is $e = 0.0818$, the earth's angular rate is $\omega_{ie} = 7.2921 \times 10^{-5}$ rad/s. The trajectory calculated by SINS is shown by a dotted cyan line in Figure 8. The data and the trajectory generated by the GPS simulator are the same as that described in Section 4.1.3. The SAR/Altimeter simulator only provided three single point positions in the middle of three particular time intervals when bias is injected into GPS, and the standard deviation was $\sigma_{SAR} = [10, 10, 10]^T$m.

The credibility of IMU was set to 100% in this simulation. The credibility of the positioning result of the SAR image matching method was 89.6% according to the results obtained in Section 4.1.2. Then, the positioning result was input into the extended Kalman filter as the measurements with adjusted variance matrix $\boldsymbol{R}_{SARc}$. The credibility of positioning result generated by the GPS simulator were evaluated according to the method described in Section 3.2. Furthermore, if the positioning results generated by the GPS simulator are reliable, they can also be fed into the Kalman filter as the measurements with adjusted variance matrix $\boldsymbol{R}_{gpsc}$. Each sensor's credibility value against time and whether or not a sensor is used in the sensor fusion loop at each time epoch are shown in Figure 10.

The trajectory of SINS/GPS/SAR fusion positioning with credibility evaluations is shown by the dashdot blue line in Figure 8. The results indicate that the accuracy of fusion positioning is improved with respect to SINS trajectory and GPS trajectory. Figures 10 and 11 describe the error and standard deviation of SINS/GPS/SAR fusion positioning results with and without credibility evaluation, respectively. It can be shown that the error of fusion positioning is nearly within 25 m in the whole trajectory and the standard deviation can correctly indicate the value of the position error. However, without a sensor credibility evaluation, the maximum error exceeds 50 m, and the standard deviation can not correctly indicate the value of the position error. It can also be observed from Figures 10 and 11 that, when GPS returns to normal from biased (for example, from 400 s to 550 s), without credibility evaluation, the final positioning error still exceeds 15 m because of the influence of the previous GPS bias. The error is larger than the standard deviation (10 m) of GPS and SAR, which indicates that it fails to fuse multi-sensors to improve the positioning accuracy. In comparison, with credibility evaluation, when GPS returns to normal, the fusion positioning error is within 5 m, and the final positioning accuracy is improved by two times.
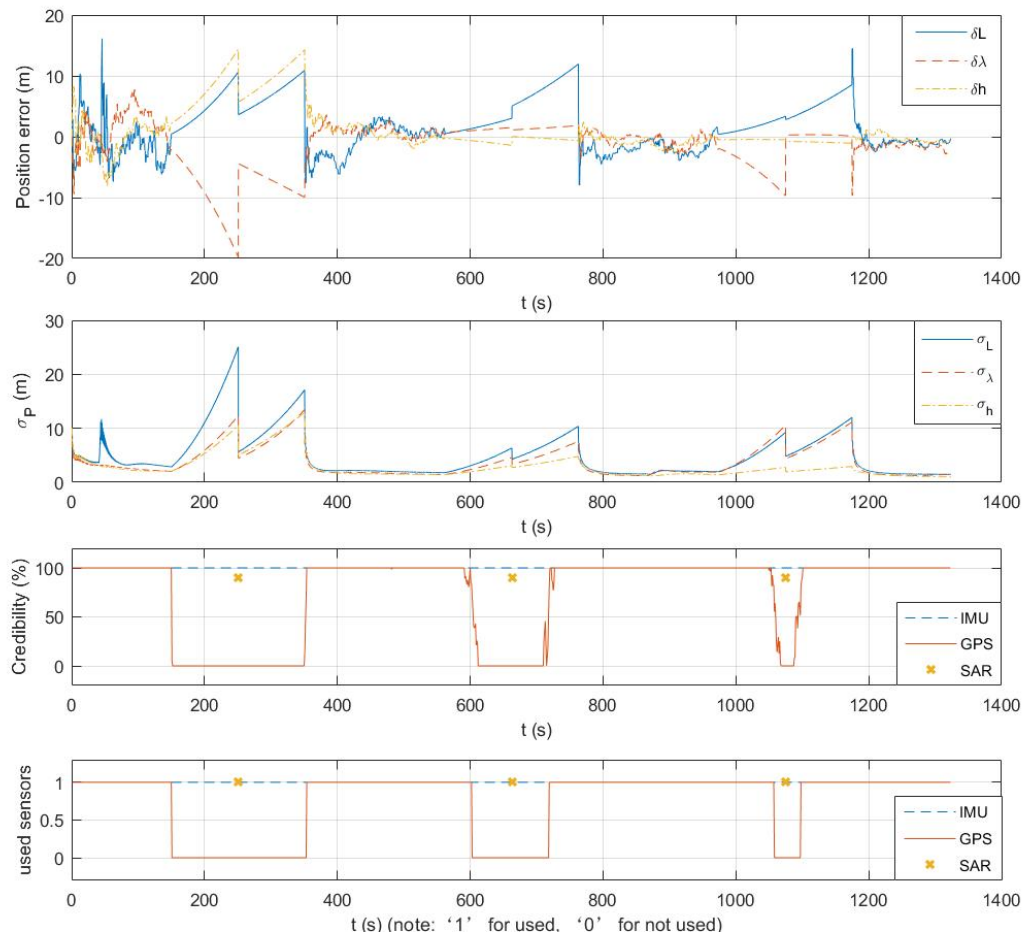
Figure 10. SINS/SAR/GPS position error and standard deviation with sensor credibility evaluation.
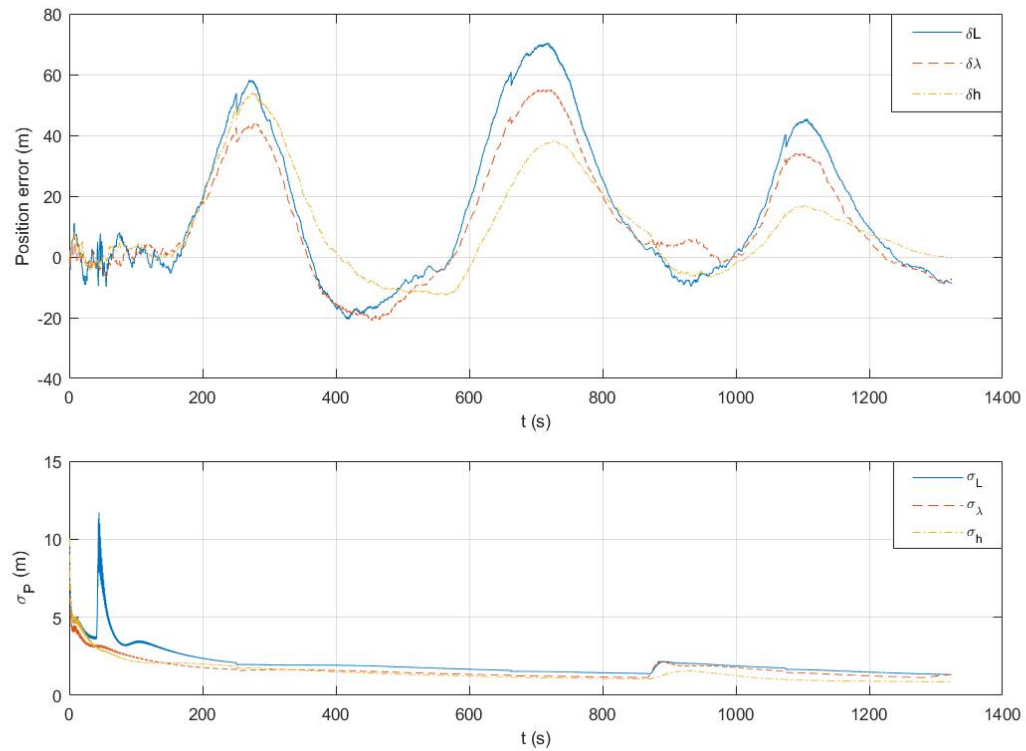

Figure 11. SINS/SAR/GPS position error and standard deviation without sensor credibility evaluation.

4.2. Experiments

To evaluate the credibility evaluation method of GPS with actual data, experiments were conducted on an unmanned ground vehicle (UGV). The UGV was equipped with a GPS receiver and runs on a highway roundabout to record GPS position data of the UGV at a frequency of 1 Hz. The precision of GPS positioning result is about 10 m when the GPS receiver is in an open and interference-free environment. A camera/IMU suite is also equipped on the UGV and is used to run a visual-inertial odometry (VIO) algorithm to obtain positioning result of the UGV. The error of the VIO's positioning result was below 10 m during the whole trajectory (about 150 s). Therefore, the result of VIO and GPS fusion positioning is accurate enough to be used as the reference of the GPS credibility evaluation. The experiment platform is shown in Figure 12.
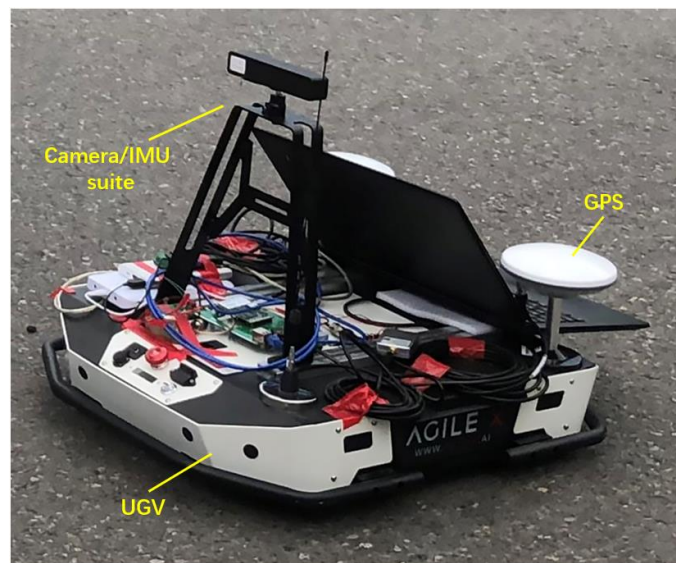

Figure 12. The UGV experiment platform.

As we conduct experiments in an open environment, the GPS interruption can only be observed in a short period of time when a car approaches the platform. Obviously, in this situation, the credibility value of the GPS is zero when it is interrupted by moving cars, and the value is 100% at other times. Therefore, we added spoofing jamming to the GPS in a period of 40 s. The trajectory of the GPS with spoofing jamming positioning is shown by the red line in Figure 13. The corresponding trajectory of the VIO positioning results is shown by the blue line in Figure 13.

Using the positioning results of the GPS with spoofing jamming and the VIO, we performed the VIO/GPS fusion positioning based on the GPS credibility evaluation (the credibility of VIO is assumed as 100%.). The trajectory of the fusion positioning results are shown by the green line in Figure 13. Comparing the trajectories of GPS, VIO, and GPS/VIO fusion, we know that the proposed fusion positioning framework based on the GPS credibility evaluation is effective. The credibility value of the GPS and the error between GPS and GPS/VIO fusion are shown in Figure 14. Comparing the error plots and the credibility plot of GPS, it can be easily found that the greater the error, the lower the credibility of the GPS, and the credibility drops to zero when the error exceeds 15 m.
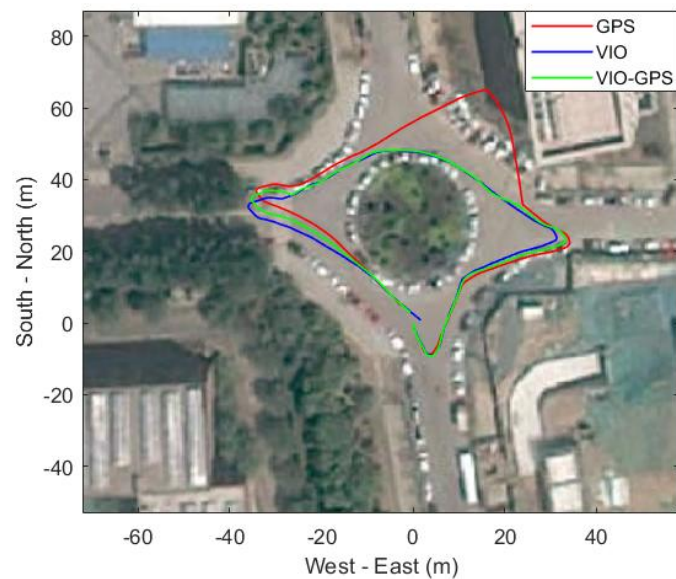
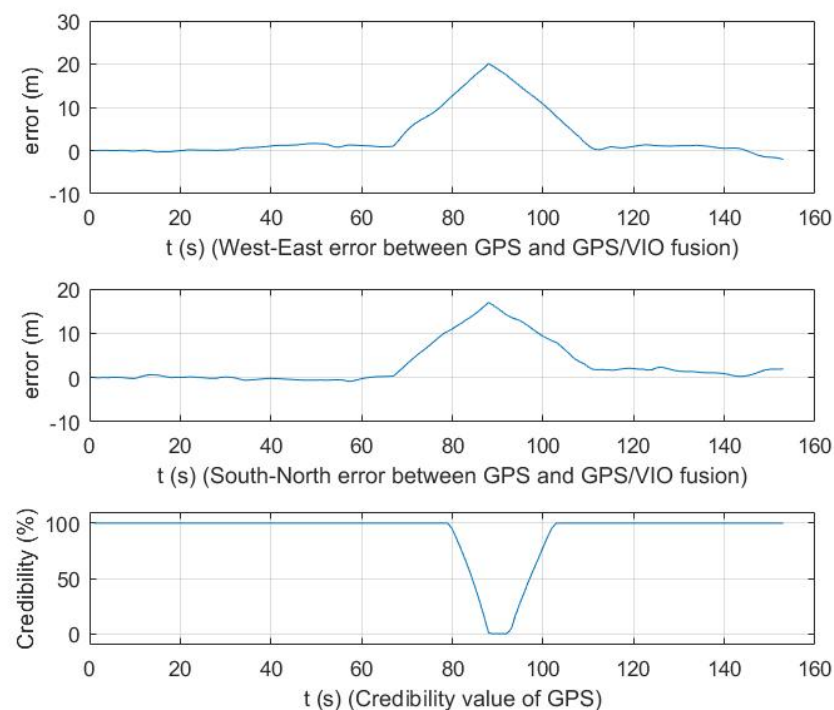**Figure 13.** 2D UGV trajectory tracking.

Figure 14. GPS error and credibility.

5. Discussion

5.1. Simulations Discussion

In the credibility evaluation for IMU simulation, we simulated the positioning error calculated by SINS, and the credibility values of the IMU were obtained. It can be observed in Figure 3 that the credibility values of IMU agree with the absolute position errors of SINS, which verifies the effectiveness of the IMU credibility evaluation method. However, the biases of gyroscopes and accelerometers cannot be totally corrected in reality. These biases will also be accumulated with time and affect the final position calculated by SINS. The details on the influence of these biases on the final position will be considered as one of our future directions.

In the credibility evaluation for SAR image matching simulation, we performed image matching between two SAR images and the matching between SAR and optical

images. The results are shown in Figures 4 and 5, and the reliability evaluation results are shown in Tables 1 and 2 . This indicates that our credibility evaluation method for SAR image matching is effective. It is also know that image matching between heterogeneous images is still an open problem. The matching of SAR and optical images often fails, as shown in Figure 6. Therefore, when evaluating the credibility of image matching between Heterogeneous images, we need to make it clear that the matching is successful, otherwise the obtained credibility value is meaningless.

In the credibility evaluation for GPS simulation, we simulate three different types of GPS spoofing biases, and successfully obtain the credibility of GPS by using the evaluation method based on a chi-square test. Note that in the daily environment, multipath and NLOS (non-line-of-sight) reception are more common interference sources than spoofing. Applying the chi-square test for the pseudorange, carrier phase, or doppler of GPS measurements can be served as a tightly-coupled solution and we will consider it as one of our future directions.

In the EKF fusion positioning based on sensor credibility simulations, we integratde the measurements and credibility values of SINS/SAR/GPS with an extended Kalman filter. Figures 10 and 11 describe the error and standard deviation of SINS/GPS/SAR fusion positioning results with and without credibility evaluation, respectively. The positioning errors are indeed enlarged when GPS is supposed to be not reliable. The reason is that only positioning results from SINS are reliable during that period and the SINS positioning error is well-known to be increasing with respect to time. However, compared with the positioning error without credibility evaluation (that is far larger than 20 m according to Figure 11), the positioning error using the proposed algorithm is within 20 m. More importantly, the standard deviation can correctly indicate the value of the position error with credibility evaluation.

The initial setting parameters of the filter are $R_{\text{gps}} = \text{diag}(\sigma_{\text{gps}})^2$, $R_{\text{SAR}} = \text{diag}(\sigma_{\text{SAR}})^2$ and $Q = \text{diag}([\varepsilon_w^b; \nabla_w^b; \mathbf{0}_{9\times1}])^2 * T_s$. The credibility of GPS is show in Figure 9 and the credibility of SAR was 89.6%. The variance matrix R used in the filter is adjusted according to the credibility value. Comparing these two figures, we can see that the fusion with credibility evaluation can improve the final positioning accuracy by 1–2 times, and the standard deviation can correctly indicate the value of the position error. We also adjusted the filter parameters to observe the affects of the filter parameters on the positioning results. In particular, we increased ε_w^b and ∇_w^b and also increased the matrix Q (that is, reducing the IMU accuracy) in 150 s–350 s, where the three credibility values of SAR in three particular time intervals were adjusted to 90%, 60%, 30%. According to the above adjusted filter parameters, the simulation results are shown in Figure 15. It can be observed from Figure 15 that, in 150 s–350 s, without GPS and SAR, the position error increases to 40 m when the the matrix Q is increased. This shows that the matrix Q (IMU accuracy) has a significant impact on the positioning accuracy when the credibility of SAR and GPS is so small that the their measurements are not trustable. It can also be observed from Figure 15 that, in 974 s–1174 s, the measurement from SAR is not used since the credibility of SAR is too small (30%), the positioning error also grows to more than 40 m at 1174 s. At about 600 s, as the GPS credibility decreases, R_{gpsc} increases, which leads to an increase of the positioning error and standard deviation. These show that the increase of matrix R (or the decrease of credibility C) will increase the positioning error.
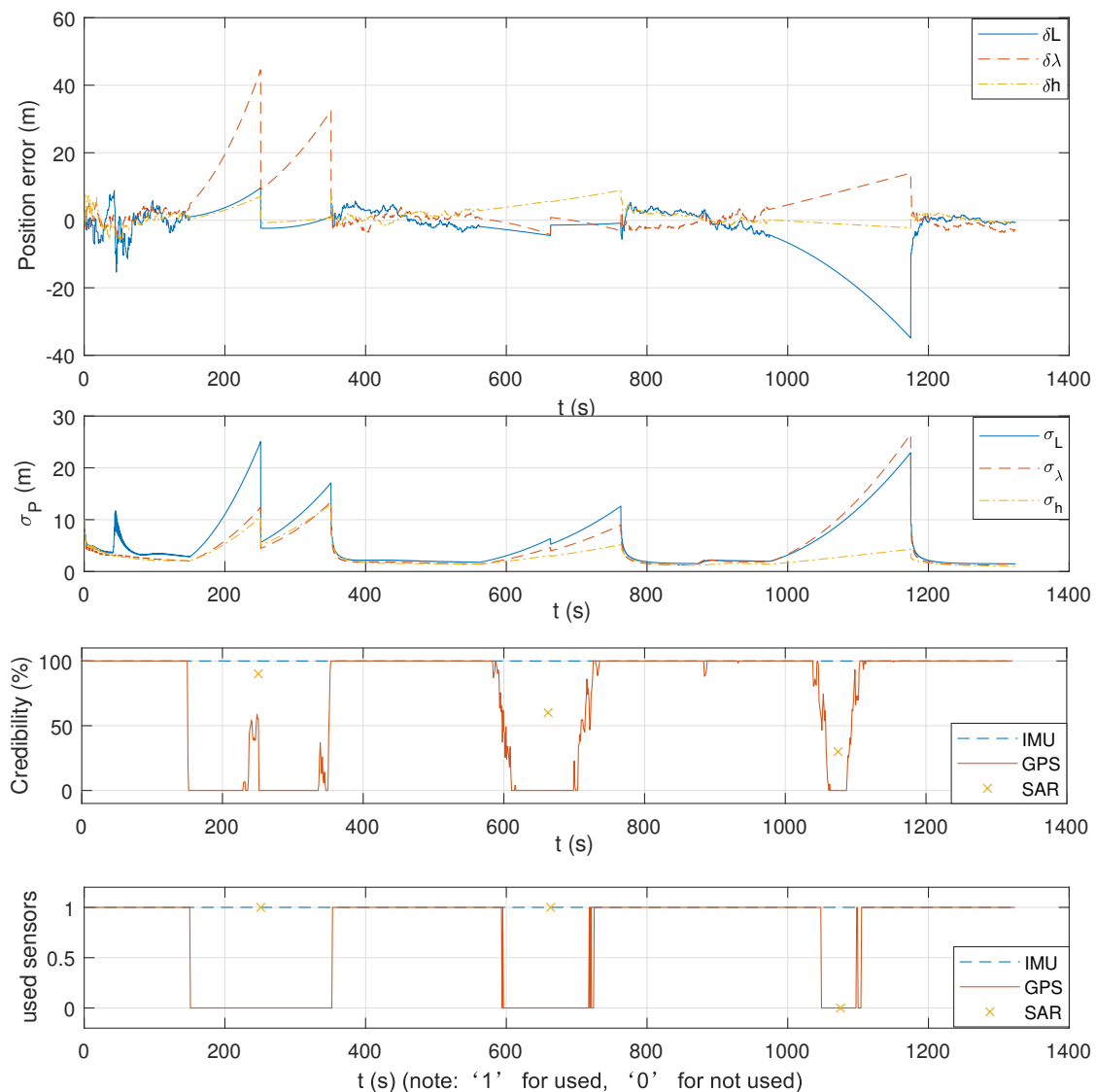
Figure 15. SINS/SAR/GPS position error and standard deviation with adjusted parameters.

5.2. Experiment Discussion

In the experiment, we used a UGV for running in a highway roundabout to record about 150 s of GPS and VIO positioning data. Besides the period of 40 s, during which we added a deception jamming to the GPS, the errors of GPS and VIO were below 10 m. Maybe the fusion results from VIO and GPS are not accurate enough to be groundtruth, but they are accurate enough to evaluate the spoofed GPS since the added deception error of GPS is nearly 30 m. The trajectories of GPS, VIO, and the fusion positioning results are shown in Figure 13, and the credibility value of the GPS and the error between GPS and GPS/VIO fusion are shown in Figure 14. Although the experiments lasted a short time, during the experiment, GPS was interfered by occasional passing cars, resulting in occasional loss of GPS positioning output. In addition, the GPS receiver was interfered with by a spoofing jammer from the attacker. Figures 13 and 14 show that the GPS credibility evaluation method and the proposed fusion positioning framework are effective.

6. Conclusions

In this work, we consider the multi-sensor fusion problem in a critical environment. The credibility evaluation methods of GPS measurements and SAR image matching method are first proposed. Then, the credibility evaluation methods of GPS and SAR are verified

by simulations. A SINS/SAR/GPS fusion framework is designed combined with sensor credibility evaluation methods. We demonstrate through simulations that, by discarding the measurement of the sensor when it is not reliable or adjusting the measurement variance matrix when it is partially reliable, the fusion with credibility evaluation can improve the final positioning accuracy by 1–2 times, and the standard deviation can correctly indicate the value of the position error with credibility evaluation. The experiments on a UGV verify the credibility evaluation of GPS and the credibility fusion framework in an actual environment. Future works will include optimizing the credibility evaluation method of each sensor and using adaptive estimation methods to better utilize the credibility of each sensor such that more accurate positioning results can be obtained.

References

1. Groves, P.D. Principles of GNSS, inertial, and multisensor integrated navigation systems. *IEEE Aerosp. Electron. Syst. Mag.* **2015**, *30*, 26–27. [CrossRef]
2. Savage, P.G. Strapdown inertial navigation integration algorithm design part 1: Attitude algorithms. *J. Guid. Control Dyn.* **1998**, *21*, 19–28. [CrossRef]
3. Savage, P.G. Strapdown inertial navigation integration algorithm design part 2: Velocity and position algorithms. *J. Guid. Control Dyn.* **1998**, *21*, 208–221. [CrossRef]
4. Gul, F.; Fang, J.; Gaho, A.A. GPS/SINS navigation data fusion using quaternion model and unscented kalman filter. In Proceedings of the 2006 International Conference on Mechatronics and Automation, Luoyang, China, 25–28 June 2006; pp. 1854–1859.
5. Wang, D.; Dong, Y.; Li, Z.; Li, Q.; Wu, J. Constrained MEMS-based GNSS/INS tightly-coupled system with robust Kalman filter for accurate land vehicular navigation. *IEEE Trans. Instrum. Meas.* **2020**, *69*, 5138–5148. [CrossRef]
6. Li, D.; Jia, X.; Zhao, J. A novel hybrid fusion algorithm for low-cost GPS/INS integrated navigation system during GPS outages. *IEEE Access* **2020**, *8*, 53984–53996. [CrossRef]
7. Fang, J.; Gong, X. Predictive iterated Kalman filter for INS/GPS integration and its application to SAR motion compensation. *IEEE Trans. Instrum. Meas.* **2009**, *59*, 909–915. [CrossRef]
8. Suri, S.; Schwind, P.; Uhl, J.; Reinartz, P. Modifications in the SIFT operator for effective SAR image matching. *Int. J. Image Data Fusion* **2010**, *1*, 243–256. [CrossRef]
9. Gao, S.; Zhong, Y.; Li, W. Robust adaptive filtering method for SINS/SAR integrated navigation system. *Aerosp. Sci. Technol.* **2011**, *15*, 425–430. [CrossRef]
10. Gao, S.; Zhong, Y.; Zhang, X.; Shirinzadeh, B. Multi-sensor optimal data fusion for INS/GPS/SAR integrated navigation system. *Aerosp. Sci. Technol.* **2009**, *13*, 232–237. [CrossRef]
11. Maier, A.; Kiesel, S.; Trommer, G. Performance analysis of federated filter for SAR/TRN/GPS/INS integration. *Gyroscopy Navig.* **2011**, *2*, 293. [CrossRef]
12. Tanıl, Ç.; Khanafseh, S.; Joerger, M.; Pervan, B. An INS monitor to detect GNSS spoofers capable of tracking vehicle position. *IEEE Trans. Aerosp. Electron. Syst.* **2017**, *54*, 131–143. [CrossRef]
13. Guo, Y.; Wu, M.; Tang, K.; Tie, J.; Li, X. Covert spoofing algorithm of UAV based on GPS/INS-integrated navigation. *IEEE Trans. Veh. Technol.* **2019**, *68*, 6557–6564. [CrossRef]
14. Narain, S.; Ranganathan, A.; Noubir, G. Security of GPS/INS based on-road location tracking systems. In Proceedings of the 2019 IEEE Symposium on Security and Privacy (SP), San Francisco, CA, USA, 19–23 May 2019; pp. 587–601.
15. Anfinsen, S.N.; Doulgeris, A.P.; Eltoft, T. Estimation of the equivalent number of looks in polarimetric synthetic aperture radar imagery. *IEEE Trans. Geosci. Remote Sens.* **2009**, *47*, 3795–3809. [CrossRef]
16. Sjanic, Z.; Gustafsson, F. Navigation and SAR focusing with map aiding. *IEEE Trans. Aerosp. Electron. Syst.* **2015**, *51*, 1652–1663. [CrossRef]

17. Yu, Q.; Zhou, S.; Jiang, Y.; Wu, P.; Xu, Y. High-performance SAR image matching using improved sift framework based on rolling guidance filter and ROEWA-Powered feature. *IEEE J. Sel. Top. Appl. Earth Obs. Remote Sens.* **2019**, *12*, 920–933. [CrossRef]
18. Rai, A.; Bhateja, V.; Bishnu, A. Speckle suppression and enhancement approaches for processing of SAR images: A technical review. In *Smart Intelligent Computing and Applications*; Springer: Singapore, 2020; pp. 695–703.
19. Papazoglou, M.; Tsioras, C. Integrated SAR/GPS/INS for target geolocation improvement. *J. Comput. Model* **2014**, *4*, 267–298.
20. Gao, S.; Xue, L.; Zhong, Y.; Gu, C. Random weighting method for estimation of error characteristics in SINS/GPS/SAR integrated navigation system. *Aerosp. Sci. Technol.* **2015**, *46*, 22–29. [CrossRef]
21. Zhao, Y.; Xiong, Z.; Tian, S.; Liu, J.; Cui, Y. INS/SAR adaptive kalman filtering algorithm based on credibility evaluation of SAR image matching results. *Acta Aeronaut. Astronaut. Sin.* **2019**, *40*, 211–222.
22. Reza, A.M. Realization of the contrast limited adaptive histogram equalization (CLAHE) for real-time image enhancement. *J. VLSI Signal Process. Syst. Signal Image Video Technol.* **2004**, *38*, 35–44. [CrossRef]
23. Derpanis, K.G. Overview of the RANSAC Algorithm. *Image Rochester NY* **2010**, *4*, 2–3.
24. Hughes, L.H.; Schmitt, M. A semi-supervised approach to sar-optical image matching. In Proceedings of the ISPRS Annals of Photogrammetry, Remote Sensing & Spatial Information Sciences, Munich, Germany, 18–20 September 2019; Volume 4.